ELSEVIER

Applied Acoustics 62 (2001) 381–409

applied acoustics

www.elsevier.com/locate/apacoust

# Insertion loss of a Helmholtz resonator in the intake system of internal combustion engines: an experimental and computational investigation

A. Selamet [a,*], V. Kothamasu [b], J.M. Novak [c]

[a] *The Ohio State University, Department of Mechanical Engineering and Center for Automotive Research, 206 West 18th Avenue, OH 43210, USA*

[b] *Arvin Exhaust, North America, 1531, 13th St., Columbus, IN 47201, USA*

[c] *Powertrain Operations, Ford Motor Company, Dearborn, MI 48121, USA*

Received 11 October 1999; received in revised form 26 February 2000; accepted 3 May 2000

**Abstract**

Wide open throttle dynamometer experiments are conducted on a firing 3.0L V6 engine with a narrow-band silencer (Helmholtz resonator) in the induction system. The effect of the silencer in the intake system is studied by performing the experiments both with and without the silencer in an intake pipe connected to a prototype intake manifold with no zip tube and air cleaner, while maintaining the overall length of the intake system. Instantaneous pressure data is acquired at key locations for a number of speeds over the operating range (1000–5000 rpm). The sound attenuation characteristics of the Helmholtz resonator are determined in terms of insertion loss. The results are presented in time-domain, as well as order-domain. The present study also describes an ongoing effort towards employing nonlinear fluid dynamic models in the time-domain for the prediction of acoustic and power performance of internal combustion engines. The model predictions compared to the experiments at a number of locations show reasonable agreement for the instantaneous pressure and sound pressure levels. 

## 1. Introduction

Pressure variation in the fresh charge of the induction system of internal combustion engines is responsible for: (1) potential "tuning" by ensuring the return of

* Corresponding author. Tel.: +1-614-292-4143; fax: +1-614-292-3163.
*E-mail address:* selamet.1@osu.edu (A. Selamet).

0003-682X/01/$ - see front matter 
PII: S0003-682X(00)00042-6

the initial rarefaction wave in the form of compression wave before the intake valve closes; and (2) generation of airborne noise which propagates to ambient through the inlet snorkel. Clearly, the former mechanism is desirable to increase the trapped fresh charge for in-cylinder combustion processes leading to improved engine torque and power output, whereas the latter is undesirable and needs to be suppressed.

The early work on the induction system of engines concentrated primarily on the tuning aspects, and therefore on the improvement of volumetric efficiency [1–6]. With the exception of Kastner [2] who performed engine dynamometer experiments on four-stroke single cylinder engines, these studies relied on simple one-dimensional linear acoustic analysis of the intake systems. Morse et al. [1], for example, employed an organ pipe analysis for the intake duct, which was then modified by Engelman and his co-workers who coupled the intake duct and the cylinder volume to resemble Helmholtz resonators. Such an approach can indicate where tuning peaks might occur over the engine speed range, and because of its simplicity, has been used extensively (see, for example, [7]). Driels [8] extended the Helmholtz approach in the frequency domain by incorporating a valve model between the cylinder volume and the intake pipe to approximate a realistic engine breathing process. Selamet et al. [9] examined the effect of distributed analysis on the resonance frequencies by comparing with the classical lumped approach.

The noise attenuation studies in the induction system of engines are relatively recent. Eversman [10] introduced the acoustic wave finite element assembly procedure to couple different elements in multiple-input, multiple-output branched systems. The technique is based on one-dimensional wave propagation combined with the source strength and impedance model at the inlet valves. In applications to four stroke four-cylinder and V8 engines, accurate predictions were obtained for the system noise output. Later, Eversman and White [11] applied a further improved version of the approach to the modeling and optimization of induction system components of a four stroke V8 engine. In addition to longitudinal propagation, transverse modes were also implemented where needed, as well as the car body transfer function to assess the noise at the driver's ear. Generating a good source model for the inherently non-linear phenomenon at the inlet valves remains, however, as a challenge for the new designs. Employing the one-dimensional wave propagation combined with acoustic experiments in an intake system driven by a speaker, Lamancusa [12] optimized the dimensions to minimize the low frequency noise transmission. Nishio and Kohama [13] proposed a pulsating simulator to evaluate intake designs with silencers in terms of volumetric efficiency and the noise reduction at the design stage. Kostun and Lin [14] studied the effect of resonator location on the sound attenuation in a simple intake system of a four-cylinder engine. Based on the modal analysis combined with a one-dimensional frequency domain approach, they showed that the resonator should be placed at or near pressure anti-nodes for effective sound attenuation.

Although Helmholtz resonator models [3,4] may help with the engine speeds for tuning, such frequency domain approach can predict neither the engine performance parameters, cam timing, and other critical design criteria, nor the time-varying amplitudes of, for example, gas pressure. To overcome this deficiency, while retaining

some of the simplicity of the frequency domain approach, Chapman et al. [15] developed an innovative approach that is based on the linearized conservation equations in the intake and exhaust ducts combined with in-cylinder thermodynamics. The method consisted of three sub-models: (1) a series of coupled nonlinear Helmholtz resonators used to describe the flow in the ducts; (2) an in-cylinder thermodynamic model; and (3) valve port boundaries that drive the system of Helmholtz resonators. Although the fluid compressibility in the ducts and the inertia in the volumes were assumed negligible, a reasonable correlation was obtained between the computational and experimental results for the single-cylinder and four-cylinder engines analyzed. While this method simplifies the duct calculations in a manner similar to linearized acoustics, it is capable of predicting the absolute magnitudes of performance parameters such as volumetric efficiency, as well as the time resolution of pressure, velocity, and density in the ducts. This approach was later extended to account for the spatial distribution by Matsumoto and Ohata [16], and Pearson and Winterbone [17] who referred to it as the "rapid wave action simulation algorithm." The extension of this technique that also accounts for the exhaust side is also known as the "hybrid" or "two-domain" approach. It is interesting to note that the frequency domain–time domain coupling has been successfully introduced earlier by Singh and Soedel [18] in treating the discharge system of reciprocating multi-cylinder compressors. Such approach has been used lately for the exhaust system of internal combustion engines with reasonable accuracy (see, for example, [19]). For a recent review on the analysis and design of silencers, the reader is referred to Munjal [20].

The time-domain approach to treat the unsteady conservation equations in the breathing system of engines is first proposed by Benson et al. [21] who employed the method of characteristics. Since then a number of other numerical techniques have been developed, including the finite difference approach of Chapman et al. [22] for engine simulation. Silvestri et al. [23], for example, also compared predictions from a commercially available time-domain model with experiments for pressure and sound pressure level in an intake system. An interesting recent example for the successful application of such a time-domain approach to production hardware is the development of Ford split port induction concept by Stockhausen et al. [24]. They essentially designed a dual runner manifold for Essex SPI engines using the input from simulation code to optimize the brake mean effective pressure and volumetric efficiency as a function of runner diameters, primary and secondary runner lengths.

The foregoing computational and experimental studies have been instrumental in the design of induction systems for engine performance and/or noise reduction. The task is challenging due to the desire to improve simultaneously the engine performance and noise reduction, particularly within the underhood space constraints of passenger vehicles. An improvement in the accuracy of predictive tools is needed to meet this challenge with the firing multi-cylinder engines. Particularly since studies of silencers with the engines have remained rather limited, further work on different type of acoustic elements in the induction system of engines is essential for reasonable prediction of sound propagation and reduction.

The objective of the present experimental and computational study is to investigate the sound attenuation behavior of *Helmholtz resonator* in the induction system. This is achieved by performing experiments on a firing 3.0L V6 engine (1) *with* the Helmholtz resonator, and (2) *without* the Helmholtz resonator in the intake system. In order to isolate the effect of silencer, the experiments are conducted with a prototype intake manifold and by eliminating the zip tube (a corrugated flexible plastic duct that connects the air cleaner box to throttle body housing) and air cleaner box in the induction system. Comparing the sound pressure level at a number of locations in the induction system reveals the insertion loss characteristics of the Helmholtz resonator. The study provides: (1) the experimental findings for crank-angle resolved gas pressure at a number of key locations in the induction system with and without the silencer elements for three selected engine speeds (low: 1000 rpm, resonance: 1780 rpm, and high: 5000 rpm); (2) the overall sound pressure levels at the same locations as a function of engine speed; and (3) half and integer orders (up to 10th order) for insertion loss characteristics of the Helmholtz resonator. The present study also employs the time-domain engine simulation model of Chapman et al. [22] for the prediction of acoustic and power performance of firing internal combustion engines. The model predictions for the pressure and sound pressure levels in the intake system are then compared to the experiments.

Following this introduction, Section 2 describes the dynamometer experiments. The insertion loss due to the Helmholtz resonator at a number of key locations in the induction system are reported in Section 3 along with the overall sound pressure levels. Section 4 compares the model predictions of the pressure and sound pressure levels to the experiment at selected locations. Finally, Section 5 ends the study with concluding remarks.

## 2. Dynamometer experiments

The wide open throttle (WOT) dynamometer experiments are conducted on a Ford 1992 3.0L V6 (Taurus) engine, which used a pair of intake systems connected to the prototype intake manifold at the throttle body as shown in Fig. 1: (1) An

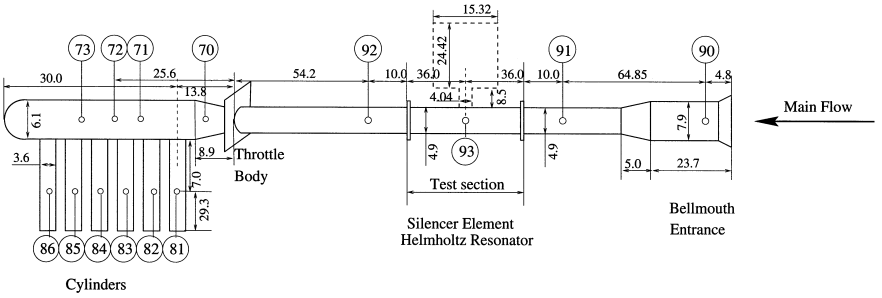


Fig. 1. 3.0L V6 Prototype intake manifold and intake system with and without the Helmholtz resonator: pressure transducer and thermocouple locations. Units are in centimetres.

"Intake system with the Helmholtz resonator", where a straight pipe with the Helmholtz resonator in the "test section" is connected to the prototype intake manifold; and (2) An "Intake system with straight pipe", where the Helmholtz resonator in the test section is replaced by a straight pipe and the overall length of the intake system is maintained. These experiments are also referred to as the intake system with and without the Helmholtz resonator. In these experiments, the zip tube and air cleaner are removed from the induction system to isolate the effect of the silencer elements. In order to minimize the effect of exhaust system elements in this study, a "Base exhaust" system with a straight pipe equal in length to the 1993 production exhaust system is used in both experiments. The primary objective of the experiments is to determine the insertion loss due to the Helmholtz resonator. The

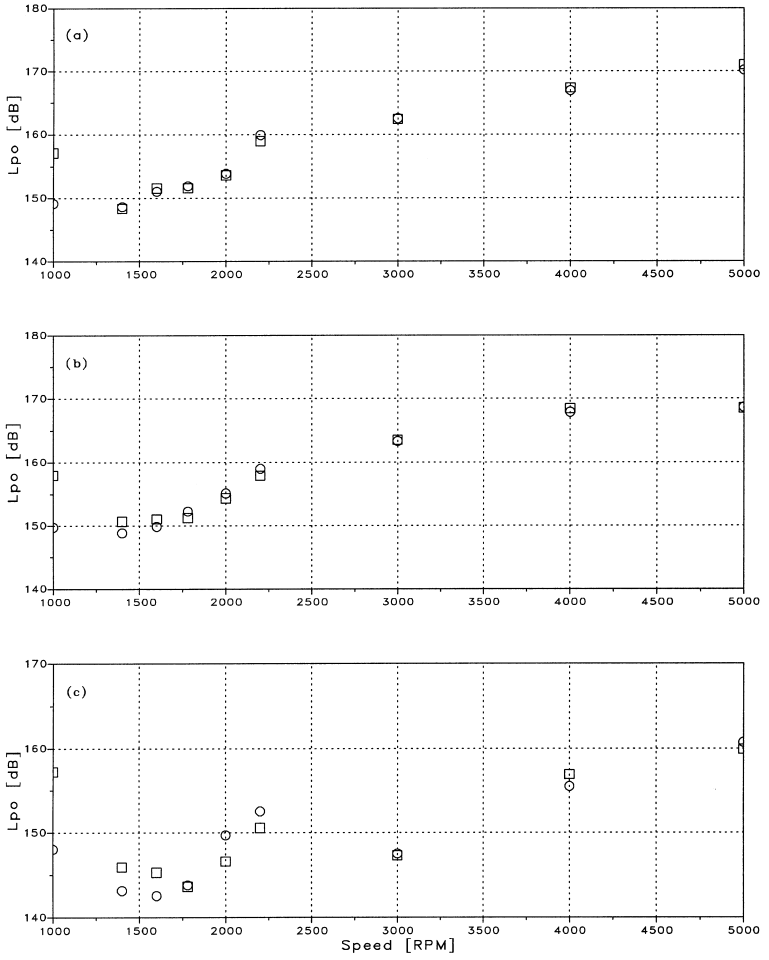


Fig. 2. Dynamometer experiment: the $L_{po}$ in the intake system with and without the Helmholtz resonator at locations (a) 81, (b) 86, and (c) 72. ○, straight pipe: □, Helmholtz resonator.

intake system is instrumented with absolute (piezoresistive) pressure transducers to quantify the insertion loss and flow losses. The numbering convention used to define the pressure measurement locations is also shown in Fig. 1. Locations 81–86 are in the primary runners, 70–72 are in the plenum of the prototype intake manifold, and 90–93 are in the "intake pipe". The intake pipe sections of different cross-sectional area are connected by gradual transitions. Consistent with the direction of air flow, the immediate upstream location of the silencer element is 91 while location 92 is the immediate downstream location. The location 93 is 180° across the pipe from the axis of the Helmholtz resonator. The intake duct connects to atmosphere with a bellmouth entrance. The engine and dynamometer facility, the steady-state and

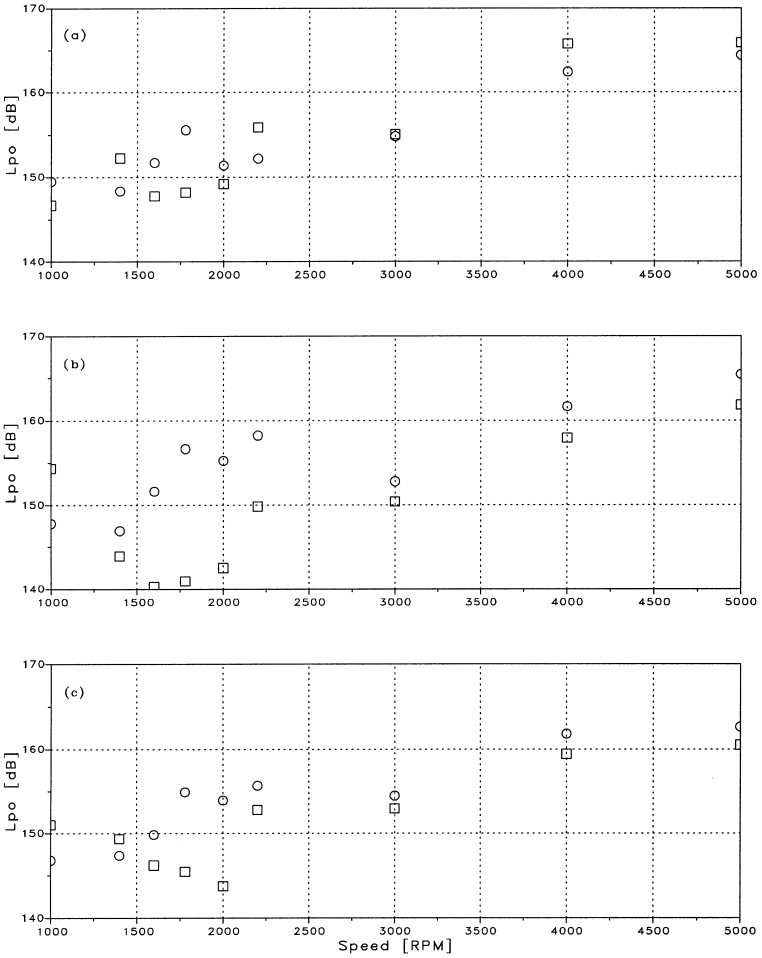


Fig. 3. Dynamometer experiment: the $L_{po}$ in the intake system with and without the Helmholtz resonator at locations (a) 92, (b) 93, and (c) 91. ○, straight pipe: □, Helmholtz resonator.

time-dependent pressure data acquisition, and the data processing are described in Ref. [25], and will not be elaborated here.

The dimensions of the narrow-band silencer, the Helmholtz resonator, used in this study are given in Fig. 1. The resonance frequency, $f_r$, for a Helmholtz resonator attached to an anechoically terminated duct with no mean flow and wavelengths much larger than any characteristic dimension is given by the lumped parameter model as

$$f_r = \frac{c_0}{2\pi}\sqrt{\frac{A_c}{l_c V}}, \tag{1}$$

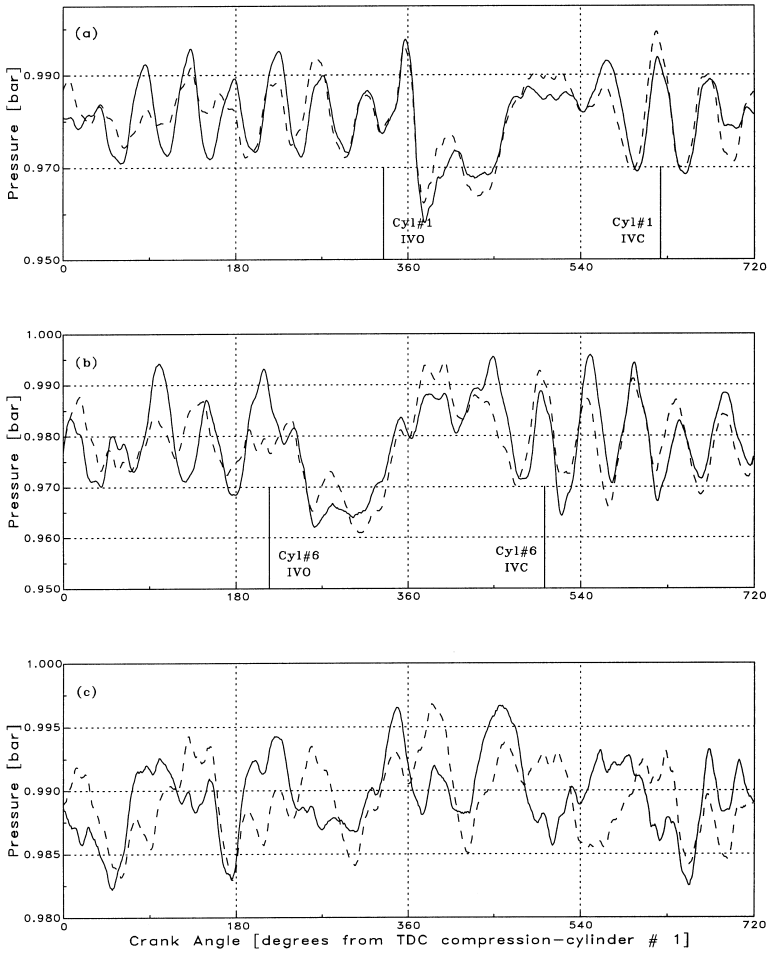


Fig. 4. Dynamometer experiment: pressure versus CAD at 1780 rpm in the intake manifold with straight pipe and Helmholtz resonator at locations (a) 81, (b) 86, and (c) 72: ———, straight pipe; — —, Helmholtz resonator.

where $c_0$ is the speed of sound, $A_c$ is the cross-sectional area of the connector (neck), $l_c$ is the connector effective length, $V$ is the resonator volume and $A_o$ is the cross-sectional area of the main duct (pipe). Experimental observations, however, usually deviate from Eq. (1) due to simplifications involved in reducing distributed, multi-dimensional phenomena to lumped parameters [9,26]. The transmission loss characteristics of the Helmholtz resonator considered in this study were investigated earlier analytically, computationally and experimentally (with an extended impedance tube) with no mean flow and anechoic termination [9], which yielded a primary resonance frequency of 89 Hz. The 3rd order of the V6 engine corresponds to the fundamental

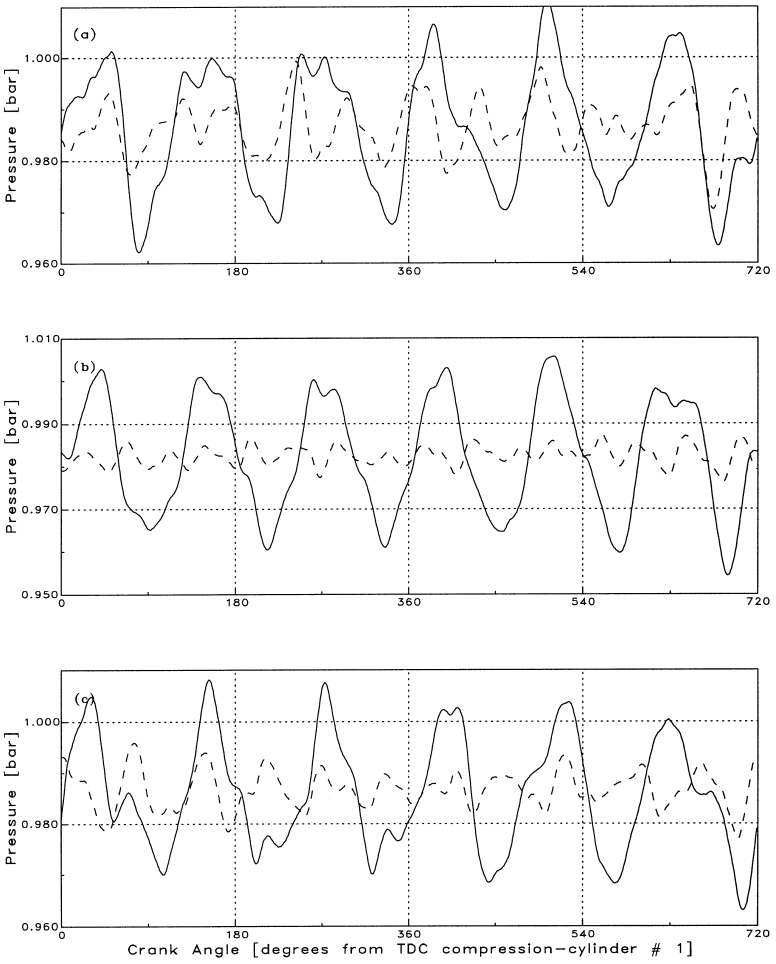


Fig. 5. Dynamometer experiment: pressure versus CAD at 1780 rpm in the intake manifold with straight pipe and Helmholtz resonator at locations (a) 92, (b) 93, and (c) 91: ——, straight pipe; — —, Helmholtz resonator.

firing frequency where maximum noise may be expected. Therefore, several engine speeds are specifically chosen around 1780 rpm ($3\times1780/60=89$ Hz) for the experiments with and without the resonator. The engine speeds for the pair of experiments with and without the Helmholtz resonator are tabulated in Table 1. The range 1000–5000 rpm corresponds to 50–250 Hz in terms of the fundamental firing frequency.

Table 1
Engine speeds in dynamometer experiments

| Intake system with and without | Engine speed (rpm) |
|---|---|
| Helmholtz resonator | 1000, 1400, 1600, 1780, 2000, 2200, 3000, 4000, 5000 |

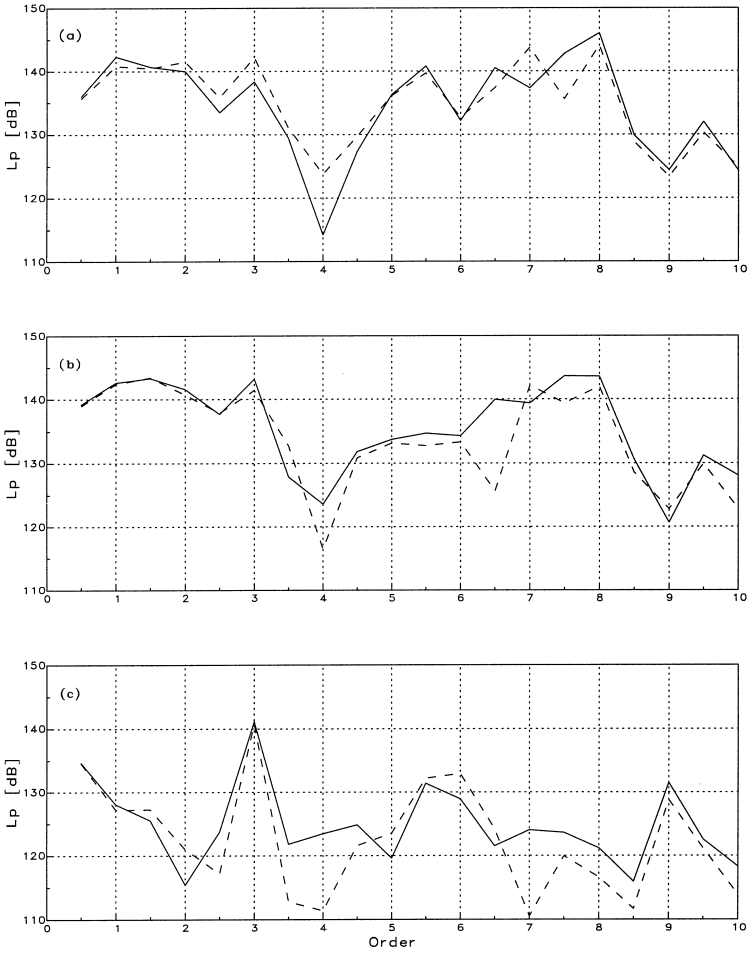


Fig. 6. Dynamometer experiment: sound pressure level versus order at 1780 rpm in the intake manifold with straight pipe and Helmholtz resonator at locations (a) 81, (b) 86, and (c) 72: ——, straight pipe; — —, Helmholtz resonator.

## 3. Insertion loss (*IL*)

The time domain pressure data may be converted to frequency/order domain information through a discrete Fourier transformation [27]. The sound pressure level in dB (decibel) for each frequency component, $L_{p,i}$, is then expressed in terms of the root mean square value of pressure as $L_{p,i} = 20 \log_{10} \frac{P_{rms,i}}{P_{ref}}$, with $P_{ref} = 2 \times 10^{-5}$ Pa. Here orders are used instead of frequencies, where $m$th order is defined as $m \times \frac{(n[\text{rpm}])}{60}$, $n$ being the engine speed. The insertion loss, *IL*, is the difference in the sound pressure levels measured at a specific location without and with the acoustic

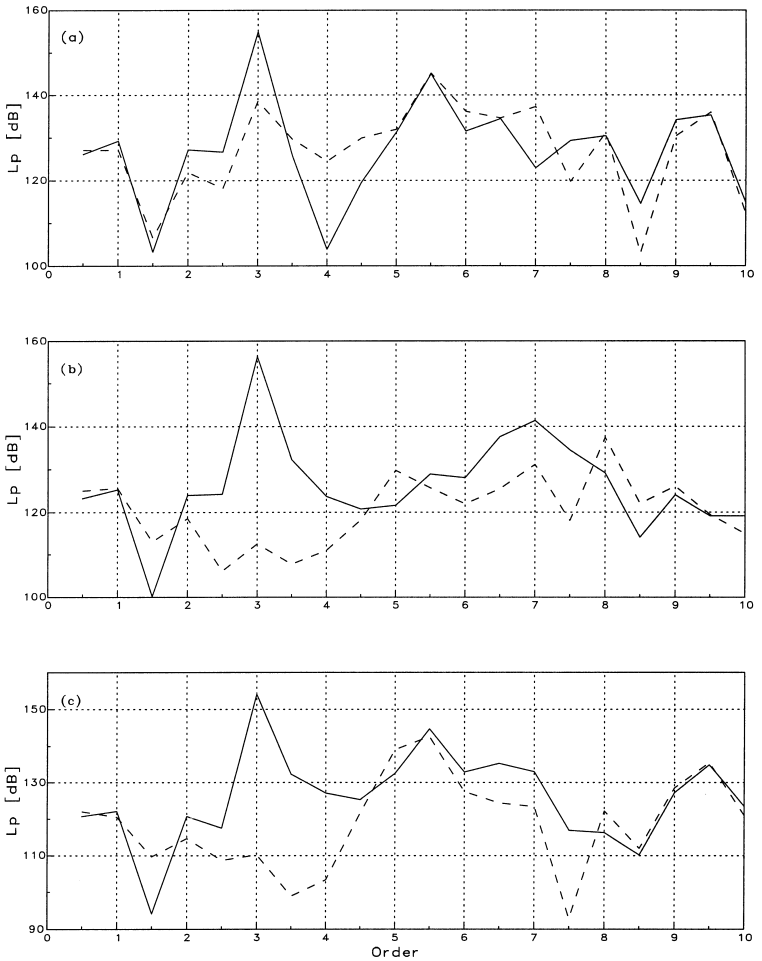


Fig. 7. Dynamometer experiment: sound pressure level versus order at 1780 rpm in the intake manifold with straight pipe and Helmholtz resonator at locations (a) 92, (b) 93, and (c) 91: ——, straight pipe; — —, Helmholtz resonator.

filter: for a specific frequency component, Insertion Loss$_i$ ($IL_i$) = $L_{\text{p,without filter}} - L_{\text{p,with filter}}$. Clearly, the same definition applies to the overall sound pressure level, $L_{\text{po}}$, as well. The locations upstream and downstream of the silencer element are defined in reference to the direction of mean fluid (air) flow and not the sound propagation.

Dynamometer experiments are conducted at various speeds from 1000 to 5000 rpm (recall Table 1) to investigate the effect of the Helmholtz resonator on the intake system. The following discussion is presented in terms of (1) the $L_{\text{po}}$ tracking with speed, and (2) the time-domain pressure traces and the corresponding $L_{\text{p}}$ which are confined to the resonance speed 1780 rpm for clarity. The results are deferred to the Appendix for the low (1000 rpm) and high (5000 rpm) engine speeds.

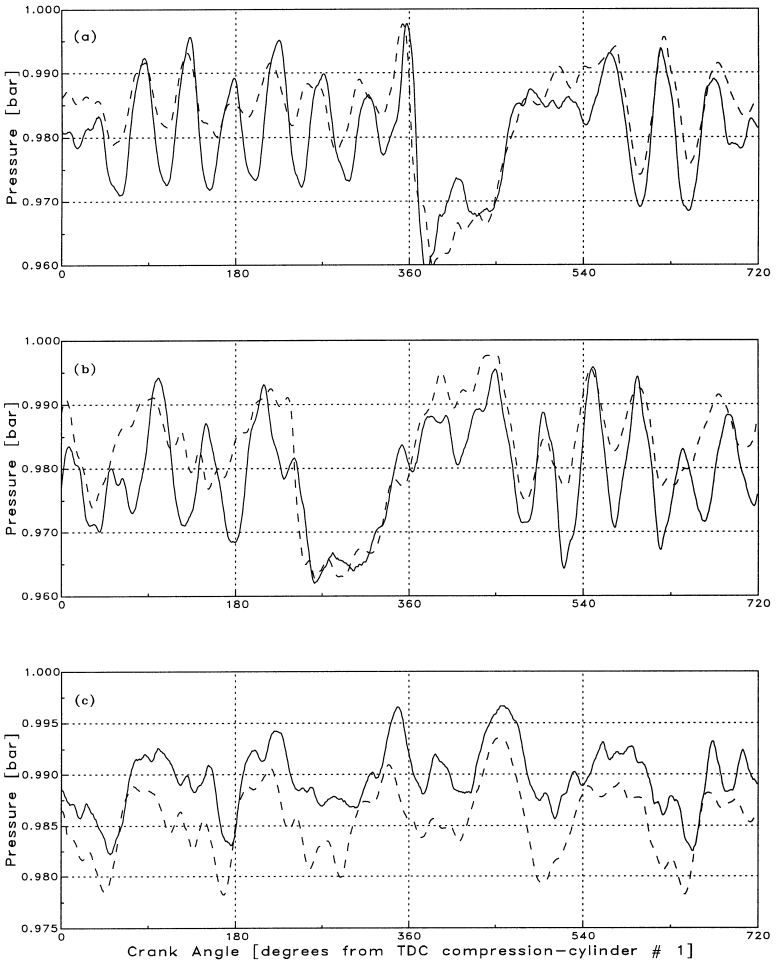


Fig. 8. Pressure versus CAD at 1780 rpm in the intake system without Helmholtz resonator at manifold locations (a) 81, (b) 86, and (c) 72: ——, experiment; — —, MANDY.

### 3.1. Overall sound pressure level tracking with speed

The $L_{po}$ as a function of speed in the intake manifold (locations 81, 86, and 72) for the system with and without the Helmholtz resonator is shown in Fig. 2. By definition, the overall IL due to the Helmholtz resonator is the difference in the $L_{po}$ with straight pipe and Helmholtz resonator. The $L_{po}$ in the intake primary runners [Fig. 2(a) and (b)] is nearly identical at all speeds except the low engine speed (1000 rpm). It is interesting to note that at 1000 rpm, the $L_{po}$ in the intake primary runners is about 8 dB higher in the intake system with Helmholtz resonator than with the straight pipe. Such behavior may be attributed to a quarter-quasi-standing wave

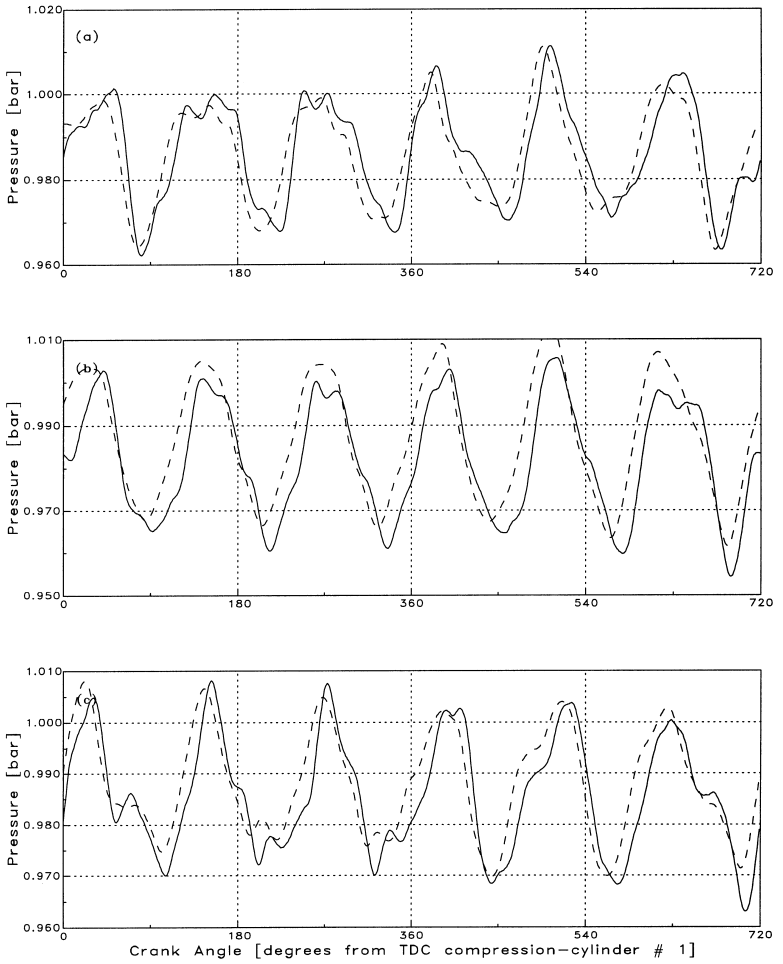


Fig. 9. Pressure versus CAD at 1780 rpm in the intake system without Helmholtz resonator at intake pipe locations (a) 92, (b) 93, and (c) 91: ——, experiment; — —, MANDY.

pattern with the introduction of resonator at that particular location and a fundamental frequency of 50 Hz, which will be shown later, in the Appendix, to be dominant at this speed. In the plenum [Fig. 2(c)], the $L_{po}$ is also higher by 10 dB with the Helmholtz resonator than with the straight pipe at 1000 rpm. The $L_{po}$ in the plenum exhibits settled differences ($\pm 2$ dB) for engine speeds 1400–2200 rpm and is nearly identical at the higher engine speeds. Thus, the effect of the resonator on $L_{po}$ (1) is negligible in the intake primary runners for all speeds, except in the neighborhood of 1000 rpm, and (2) persists in the plenum to an extent beyond 1000 rpm.

The $L_{po}$ as a function of engine speed in the intake pipe (locations 91–93) for the system with and without the Helmholtz resonator is shown in Fig. 3, which clearly reveals the characteristics of a narrow-band resonator. At the downstream location

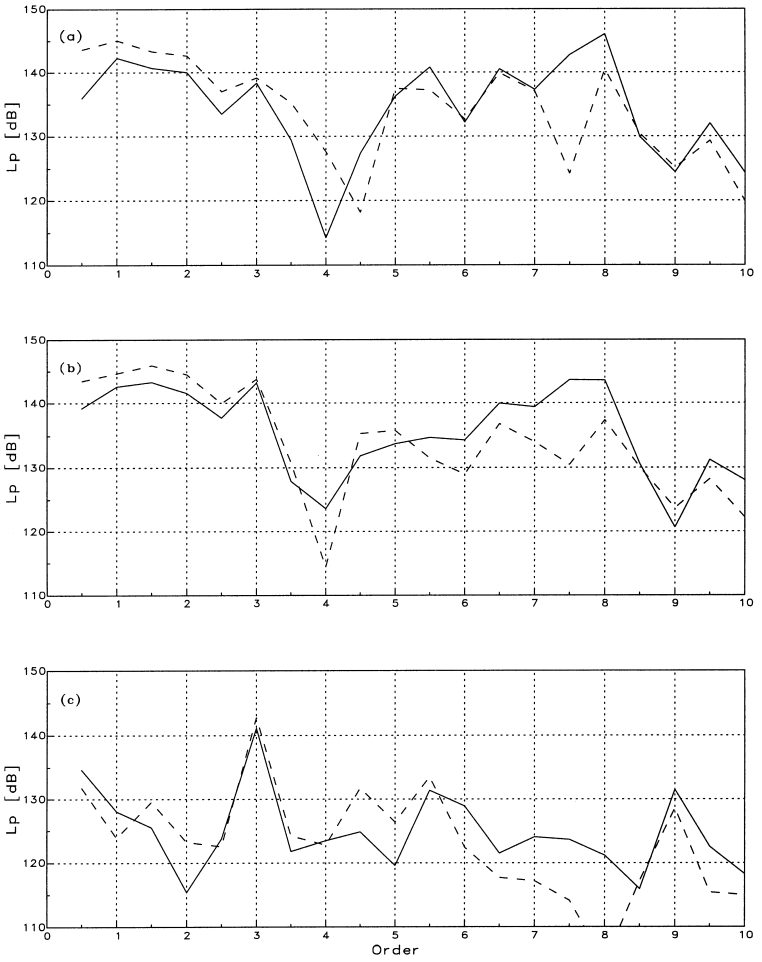


Fig. 10. Sound pressure level versus order at 1780 rpm in the intake system without Helmholtz resonator at manifold locations (a) 81, (b) 86, and (c) 72: ——, experiment; — —, MANDY.

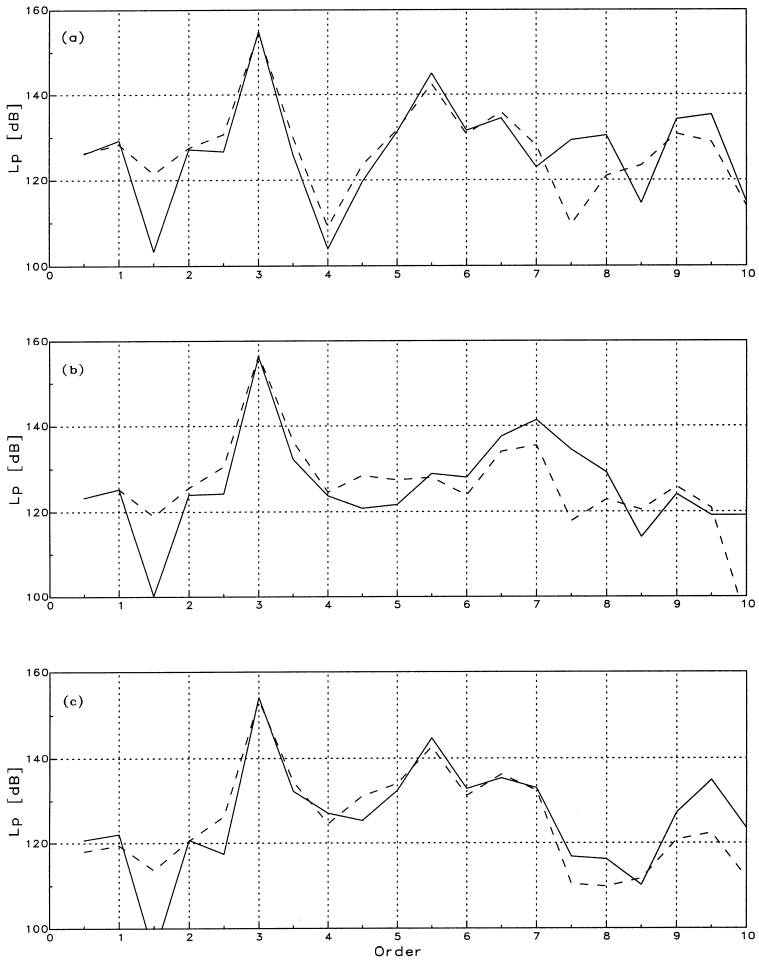


Fig. 11. Sound pressure level versus order at 1780 rpm in the intake system without Helmholtz resonator at intake pipe locations (a) 92, (b) 93, and (c) 91: ——, experiment; — —, MANDY.

92 [Fig. 3(a)], the $L_{po}$ increases with the insertion of resonator for all speeds, except for speeds of 1600–2000 and 1000 rpm. Except for 1000 rpm, the IL is positive for all speeds at location 93 [Fig. 3(b)]. At this neck location, the $L_{po}$ reduction with resonator is maximum at 1780 rpm (16 dB), and decreases with speed on either side in the range 1400–2200 rpm. Thus, at the resonance frequency, the present narrow band silencer produces a quasi[1]-pressure node. At higher engine speeds (3000 rpm on or away from the resonance frequency), the IL is within 4 dB. At the important

[1] The pressure fluctuations at this point are nowhere near negligible, thus the location is not a pressure node as defined in the classical sense. However, pressure amplitude at this point is significantly lower than no-resonator case, thereby lending to the terminology "quasi-node".

upstream location 91 [Fig. 3(c)], the $L_{po}$ reduction is significant only for engine speeds around 1780 rpm. The $L_{po}$ attenuation is slightly negative for 1000 and 1400 rpm (within −3 dB), nearly negligible (about 2 dB) at the high engine speeds (3000, 4000, and 5000 rpm), and within 10 dB for engine speeds near 1780 rpm. Thus, the effect of the Helmholtz resonator on $L_{po}$ at the immediate downstream and upstream locations is most pronounced near the tuned engine speed or frequency.

### 3.2. Intake wave dynamics: straight pipe versus Helmholtz resonator

The comparison of pressure versus crank angle in the intake system with and without the Helmholtz resonator at 1780 rpm for the same locations of the preceding

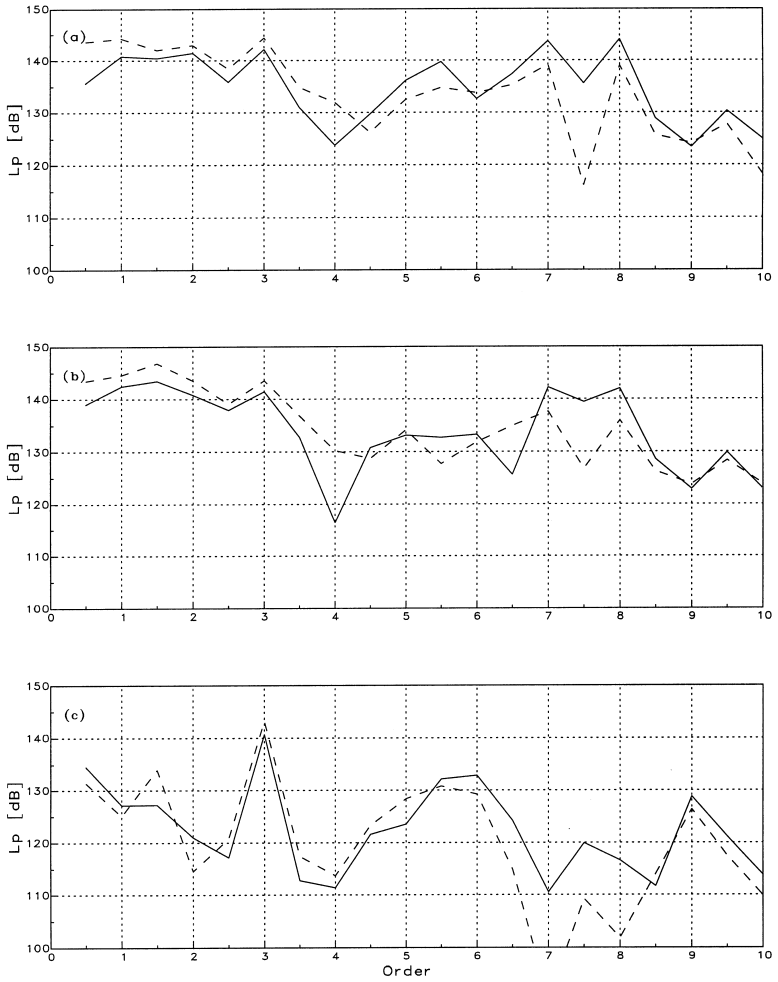


Fig. 12. Sound pressure level versus order at 1780 rpm in the intake system with Helmholtz resonator at manifold locations (a) 81, (b) 86, and (c) 72: ——, experiment; — —, MANDY.

section is shown in Figs. 4 and 5. Also included in Fig. 4(a) and (b) are the intake valve opening (IVO) and closing (IVC) events for cylinder #1 and #6. In the intake primary runners [Fig. 4(a) and (b)], the phasing of peaks and valleys of the pressure wave, in general, remain the same, but the pressure amplitudes exhibit some differences. Unlike the primary runners, in the plenum [location 72, Fig. 4(c)] the pressure wave form and amplitude is different with the Helmholtz resonator. The pressure wave amplitude in the intake pipe (locations 91–93, Fig. 5) is lower in the intake system with Helmholtz resonator than with straight pipe. The reduction in pressure amplitude is maximum at location 93. Thus, the insertion of the Helmholtz resonator changes the pressure wave form significantly in the intake pipe at the engine speed with fundamental firing frequency corresponding to the resonance frequency

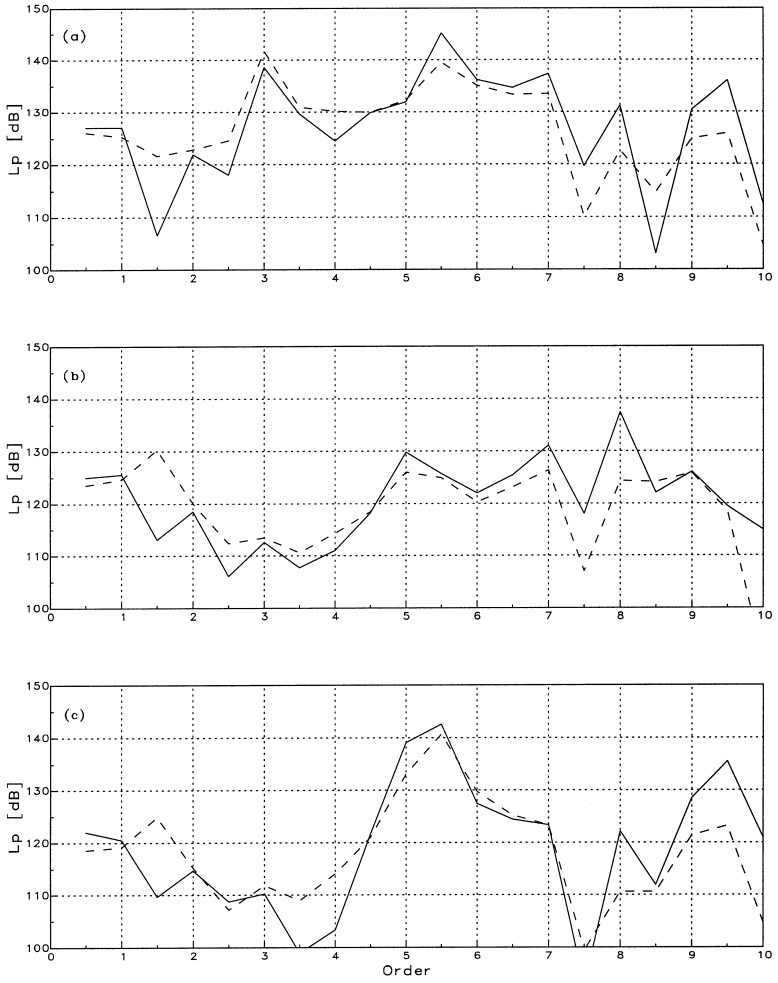


Fig. 13. Sound pressure level versus order at 1780 rpm in the intake system with Helmholtz resonator at intake pipe locations (a) 92, (b) 93, and (c) 91: ——, experiment; — —, MANDY.

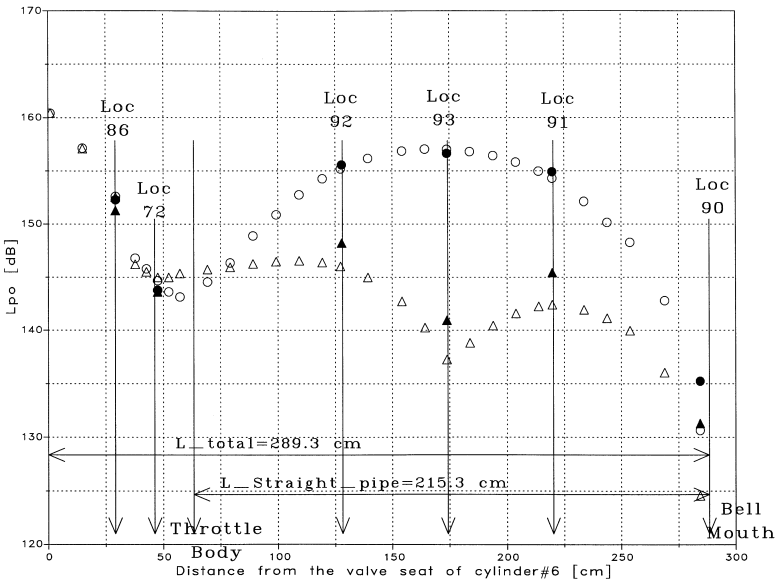


Fig. 14. Comparison of $L_{po}$ in the intake system for the straight pipe and Helmholtz resonator between the experimental and computational model at 1780 rpm: ●, experiment: straight pipe; ○, MANDY: straight pipe; ▲, experiment: Helmholtz resonator; △, MANDY: Helmholtz resonator.

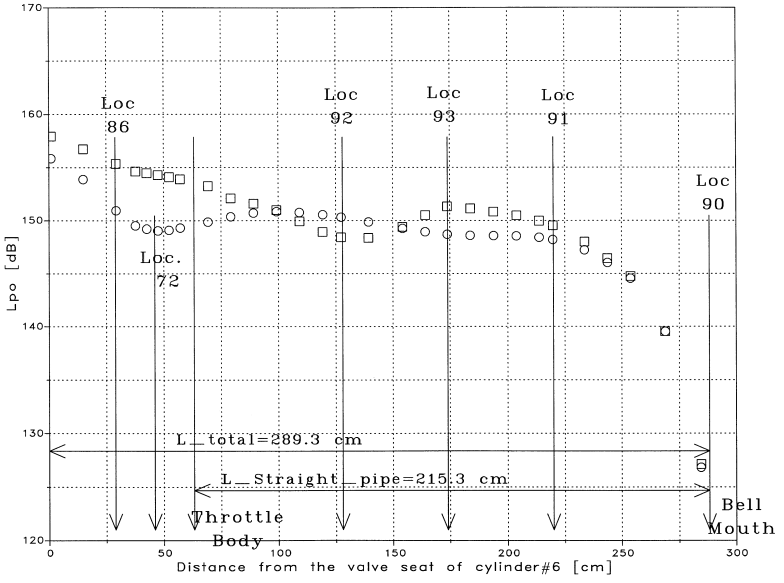


Fig. 15. Computational model (MANDY) prediction of $L_{po}$ in the intake system for the straight pipe and Helmholtz resonator at 1000 rpm: ○, straight pipe; □, Helmoholtz resonator.

of resonator; while the impact in primary runners is not nearly as significant. Also, worth noting in primaries [Fig. 4(a) and (b)] is the period, $T$, of pressure waves being closely represented by $T = \frac{4l_{\text{primary}}}{c_0}$ during the valve closed period, $l_{\text{primary}}$ being the length between the valve and the plenum. This is not surprising in view of the fact that when intake valve is closed, the duct between the valve and the plenum could be approximated as closed on one end and open at the other with relatively small bulk motion.

The sound pressure level versus order for the first several half and integer orders (up to 10th order) corresponding to the pressure-time data of Figs. 4 and 5 is given in Figs. 6 and 7. The $L_p$ in the intake primary runners [Fig. 6(a) and (b)] shows some

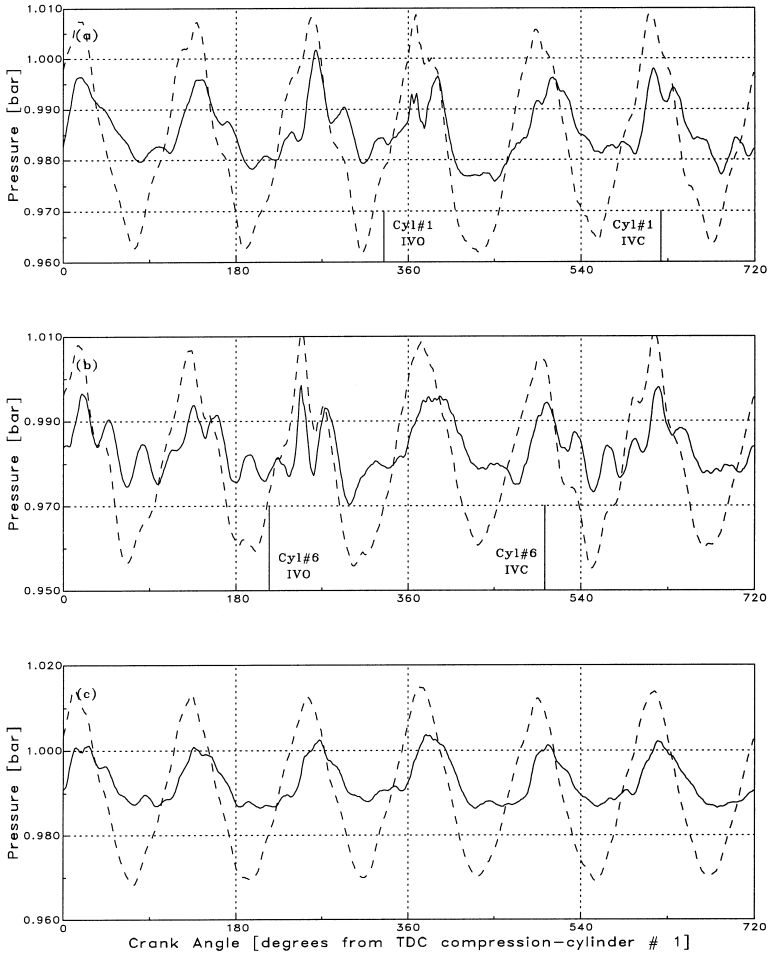


Fig. 16. Dynamometer experiment: pressure versus CAD at 1000 rpm in the intake manifold with straight pipe and Helmholtz resonator at locations (a) 81, (b) 86, and (c) 72: ——, straight pipe; — —, Helmholtz resonator.

variation with and without the Helmholtz resonator. The $L_p$ for the dominant 3rd order in the plenum [Fig. 6(c)] is transparent to the presence of the Helmholtz resonator, while the *IL* for other orders exhibit some fluctuations. Thus, the effect of the Helmholtz resonator is not substantial in the intake manifold. This fact is also reflected in the summed information ($L_{po}$), as well as the pressure traces discussed earlier in Section 3.1 (see Fig. 2). The $L_p$ versus order in Fig. 7 for the intake pipe locations 92, 93, and 91 clearly demonstrates the effect of Helmholtz resonator on the sound attenuation in the intake system. At these locations of the straight intake system (solid line of Fig. 7), the $L_p$ of the 3rd order dominates. Introducing the Helmholtz resonator reduces the $L_p$ of the 3rd order at all locations in the intake pipe. The *IL* for the 3rd order exceeds 40 dB at locations 93 and 91. Thus, comparing

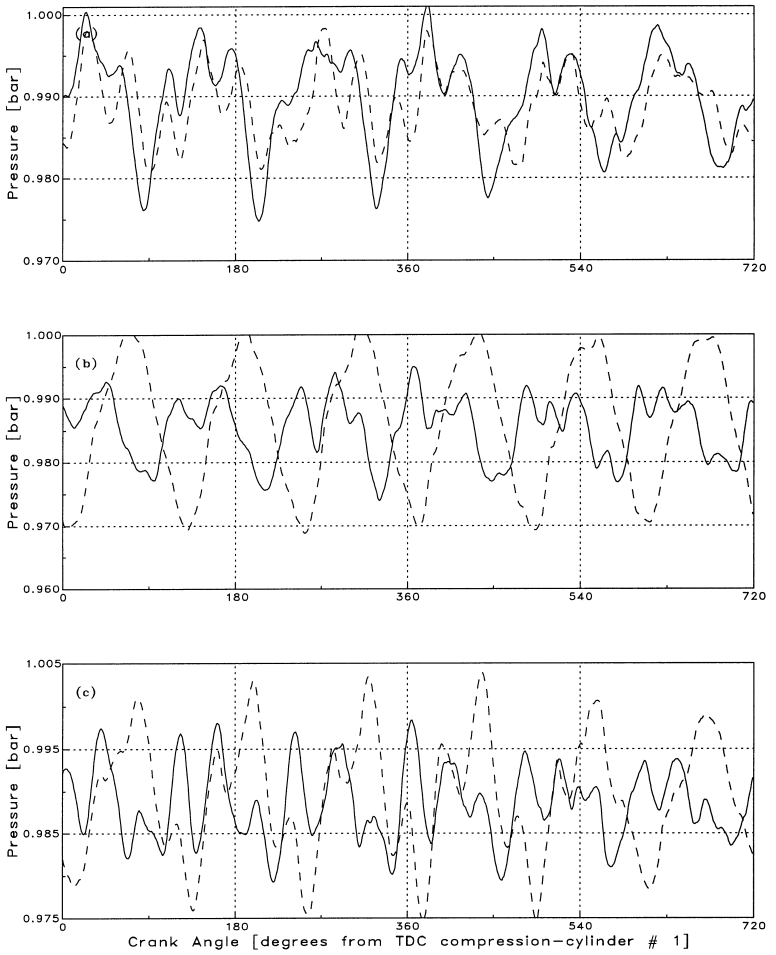


Fig. 17. Dynamometer experiment: pressure versus CAD at 1000 rpm in the intake manifold with straight pipe and Helmholtz resonator at locations (a) 92, (b) 93, and (c) 91: ——, straight pipe; — —, Helmholtz resonator.

the $L_p$ in the intake system with and without the Helmholtz resonator reveals a very effective $L_p$ attenuation at the upstream location and an insignificant impact of the resonator in the intake manifold.

## 4. Computational approach

The numerical technique is a quasi one-dimensional time domain approach to solve the balance equations for mass, momentum, and internal energy in ducts of variable cross section. These relationships are discretized by employing the explicit

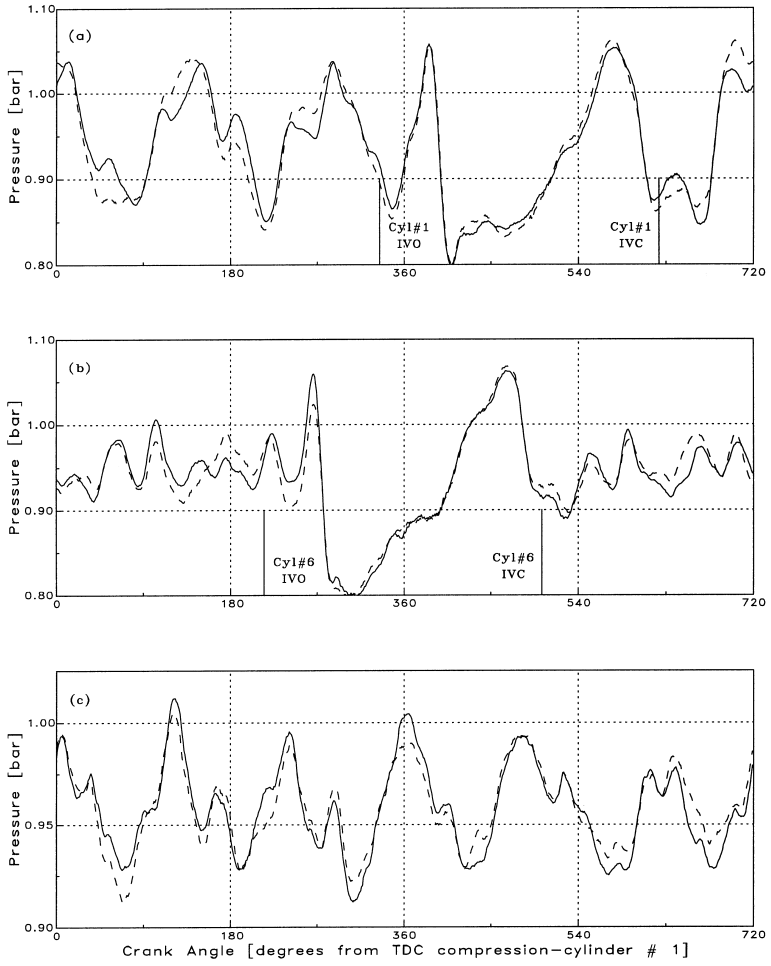


Fig. 18. Dynamometer experiment: pressure versus CAD at 5000 rpm in the intake manifold with straight pipe and Helmholtz resonator at locations (a) 81, (b) 86, and (c) 72: ——, straight pipe; — —, Helmholtz resonator.

finite difference method of Chapman et al. [22] as discussed by Selamet et al. [28]. The staggered mesh used in the discretization divides a duct into cells with vector quantities located at node points and scalar quantities at cell midpoints. The ideal gas equation of state is used to relate the thermodynamic variables and close the system of equations. Intake and exhaust ports communicate with incylinder physics during valve-open periods. In-cylinder physics is based on the first law of thermodynamics combined with heat release and heat transfer models as described in Ref. [22]. The predictions presented in this study use a grid size of $\Delta x = 0.5$ cm.

The model predictions for the time-domain pressure and the corresponding $L_p$ are presented next for a selected engine speed, 1780 rpm, in the intake system without

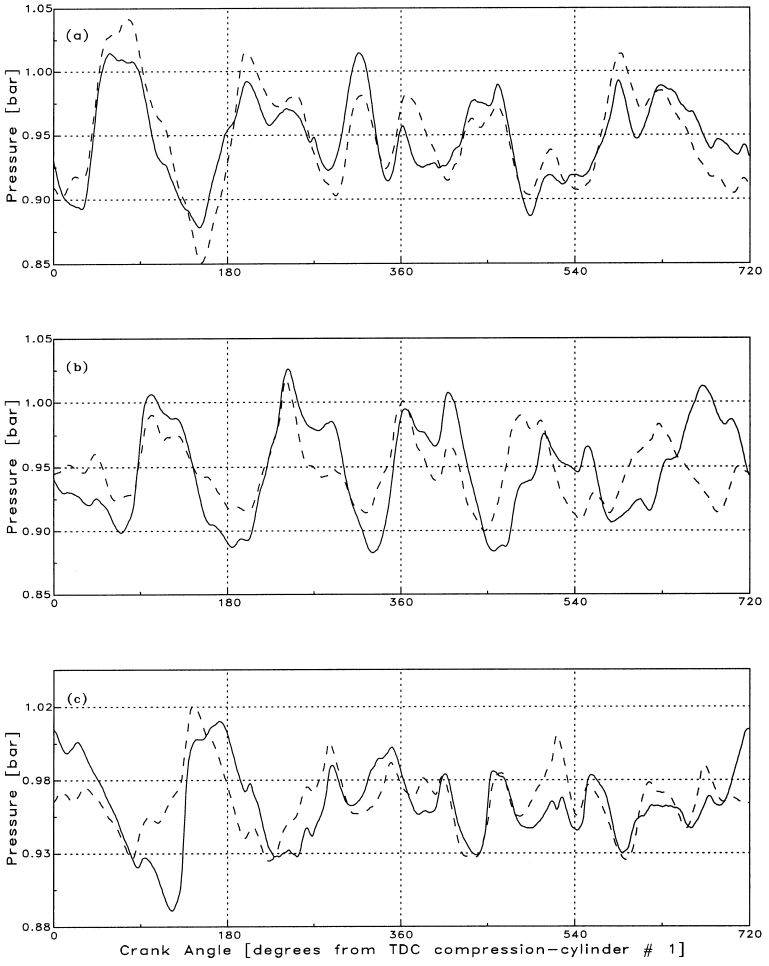


Fig. 19. Dynamometer experiment: pressure versus CAD at 5000 rpm in the intake manifold with straight pipe and Helmholtz resonator at locations (a) 92, (b) 93, and (c) 91: ——, straight pipe; — —, Helmholtz resonator.

the silencer element. Figs. 8 and 9 compare the experiments and predictions for the pressure variation in the intake system without the Helmholtz resonator at 1780 rpm. The model predictions are reasonable for the phasing of peaks and valleys in the intake manifold (Fig. 8) as well as the intake pipe locations (Fig. 9), while the predicted amplitudes exhibit settled differences. The $L_p$ corresponding to the pressure-time data of Figs. 8 and 9 is shown in Figs. 10 and 11. In the intake primary runners, the model predicts the relative contribution of various orders, in general, reasonably well; however, the predicted $L_p$ may, at times, deviate from the experiments (for example, at $7\frac{1}{2}$ order). In the plenum, the model predicts the important orders (3rd, $5\frac{1}{2}$, and 9th) reasonably well. Both predictions and experiments show the dominance of 3rd order in the intake pipe, and the deviation of predictions from

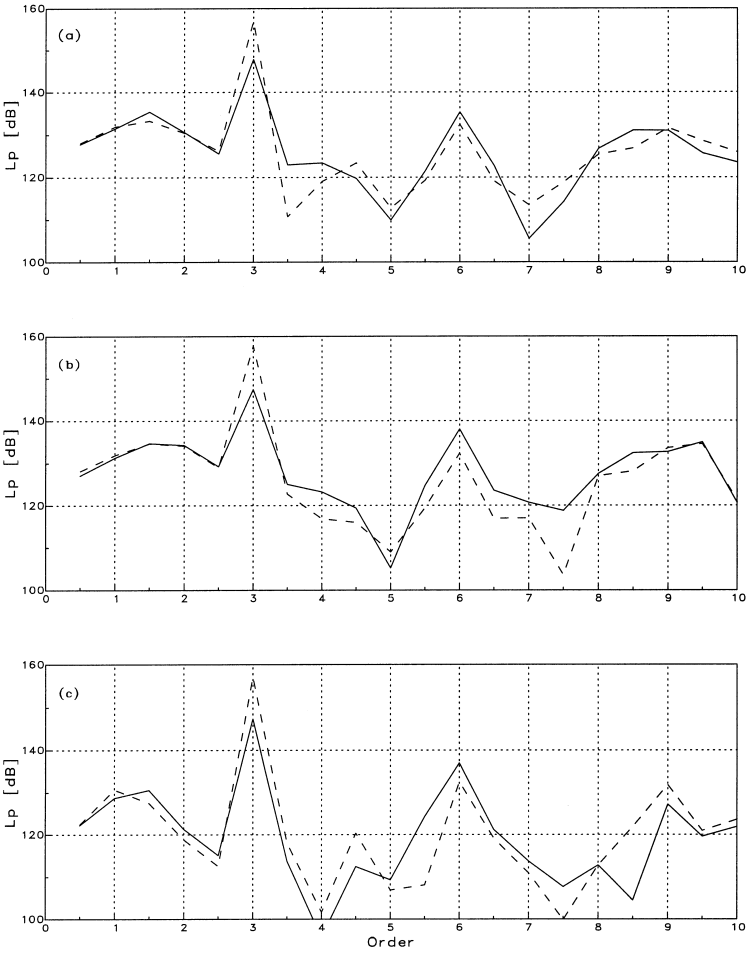


Fig. 20. Dynamometer experiment: sound pressure level versus order at 1000 rpm in the intake manifold with straight pipe and Helmholtz resonator at locations (a) 81, (b) 86, and (c) 72: ——, straight pipe; — —, Helmholtz resonator.

experiments at other insignificant orders (in terms of contribution to magnitude) may be ignored.

Figs. 12 and 13 compare the $L_p$ predictions and experiments in the intake system with the Helmholtz resonator. The model predictions for the relative contribution of various orders in the intake manifold is, in general, reasonable. In the intake pipe locations 92, 93, and 91, the model predicts the important orders well, while exhibiting some deviation at few orders such as $1\frac{1}{2}$ and 8th.

The experimental and computational results for the $L_{po}$ in the intake system are compared in Fig. 14 with and without the resonator. In addition to symbols representing the experimental results, key transducer locations are also designated by

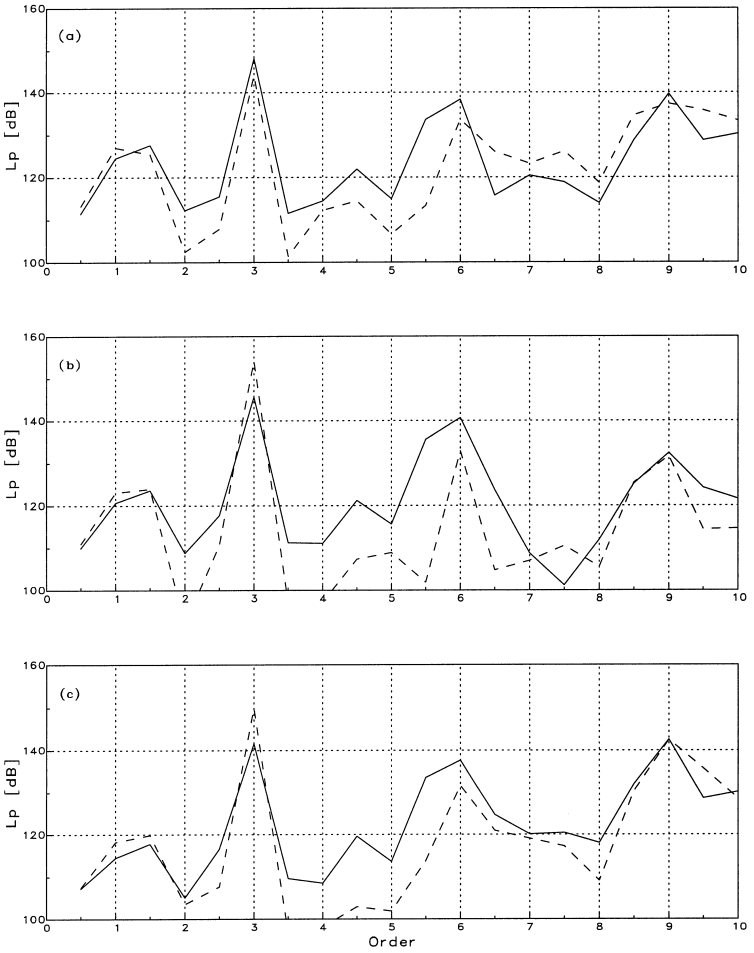


Fig. 21. Dynamometer experiment: sound pressure level versus order at 1000 rpm in the intake manifold with straight pipe and Helmholtz resonator at locations (a) 92, (b) 93, and (c) 91: ——, straight pipe; — —, Helmholtz resonator.

vertical bars. The computational model predicts the $L_{po}$ in the intake system with straight pipe rather accurately. The predictions are somewhat lower than the experimental data for the Helmholtz resonator. The variation is less than 4 dB in the intake pipe for locations 91, 92, and 93 and about 3 to 7 dB at the bellmouth entrance. Fig. 14 reveals the amplitude pattern as a function of location (shape of quasi-standing wave), as well as the impact of silencer on this pattern. Note how significantly the oscillations are modified by the insertion of the silencer, including the drastic suppression of amplitudes at location 93. Fig. 15 shows the predictions for $L_{po}$ in the intake system with and without the Helmholtz resonator at 1000 rpm which exhibited a significant increase in $L_{po}$ (recall Fig. 2) particularly in exhaust

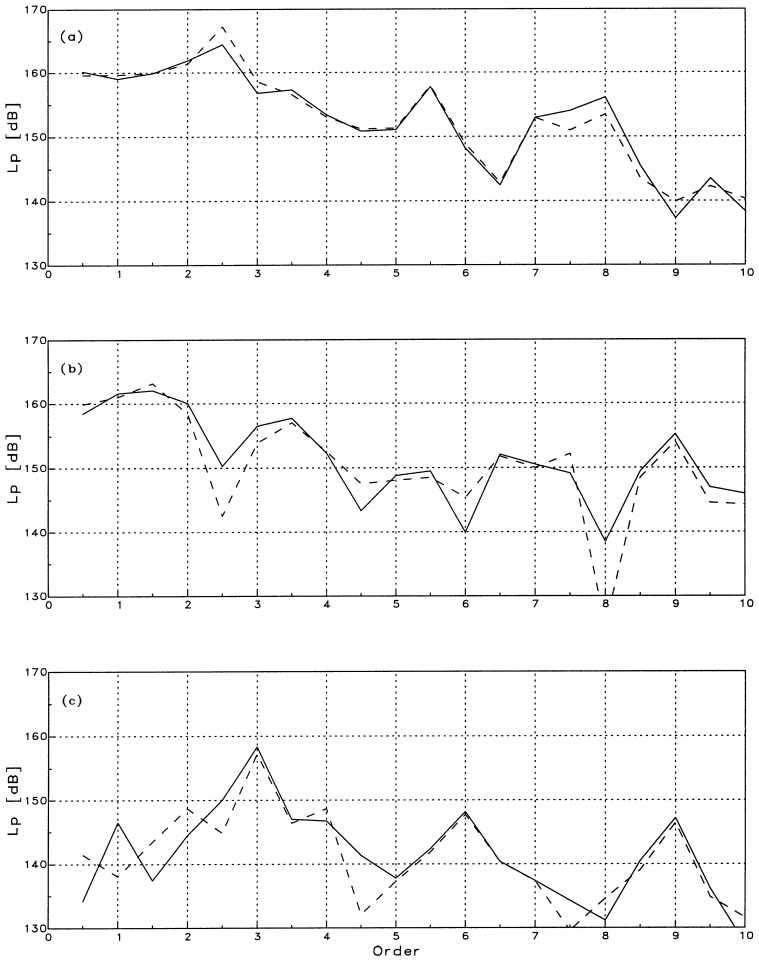


Fig. 22. Dynamometer experiment: sound pressure level versus order at 5000 rpm in the intake manifold with straight pipe and Helmholtz resonator at locations (a) 81, (b) 86, and (c) 72: ——, straight pipe; — —, Helmholtz resonator.

primaries. Note that the insertion of resonator in the intake system at 1000 rpm causes a near quarter-wave between the intake valve and the quasi-pressure node in the vicinity of location 92, leading to a crossing pattern and higher amplitudes on either side, including the primary runner location 86. These predictions are consistent with and shed further light on the low speed experimental results discussed in the preceding sections involving Figs. 2 and 3, as well as those to be elaborated further in the Appendix.

The foregoing comparisons demonstrate the ability of the time-domain model to predict the pressure wave form and amplitudes, the significant orders of the spectrum contributing to the $L_{po}$, and the $L_{po}$ in the entire intake system. While the

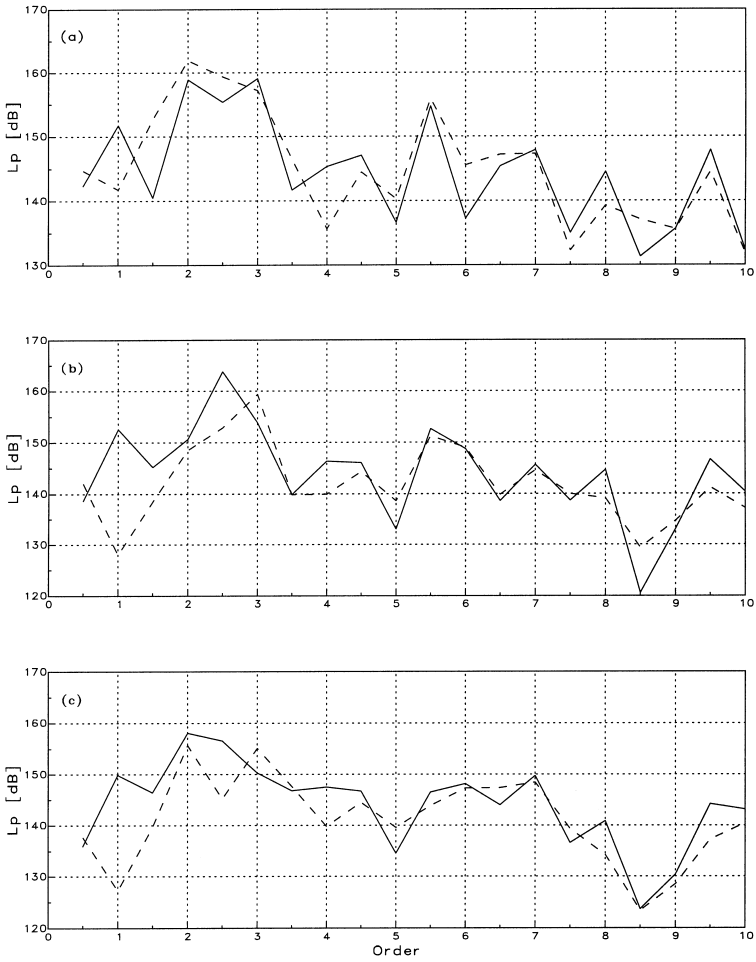


Fig. 23. Dynamometer experiment: sound pressure level versus order at 5000 rpm in the intake manifold with straight pipe and Helmholtz resonator at locations (a) 92, (b) 93, and (c) 91: ——, straight pipe; — —, Helmholtz resonator.

sources of deviation are currently under investigation for further improvement, it is known, for example, that the accuracy of the predictions increases with the reduction in grid size [9].

## 5. Concluding remarks

The insertion loss characteristics of a narrow-band silencer (Helmholtz resonator) are studied experimentally and computationally in the induction system of a firing 3.0L V6 internal combustion engine. The influence of the Helmholtz resonator in the induction system is demonstrated by using the time-domain pressure and the corresponding $L_p$ data at key locations with and without the resonator in the system. The narrow-band nature of the sound attenuation of the resonator is clearly demonstrated by the significant overall IL at engine speeds with fundamental firing frequency near the resonance frequency and insignificant reduction at other speeds. With the exception of 1000 rpm, the intake primary runners are found to be nearly insensitive to the presence of the Helmholtz resonator. The impact of the resonator on the volumetric efficiency and therefore torque is hardly noticeable (within less than 2%) at engine speeds with fundamental firing frequency near the resonance frequency. While the grazing flow in the main duct is usually recognized to reduce/deteriorate the sound attenuation performance of Helmholtz resonators [29], and may lead to flow-acoustic coupling at discrete Strouhal numbers [30], no attempt is made here to investigate this phenomenon, except to observe that the resonator functions effectively at the design frequency and no unusual pure tones are measured as an evidence of flow acoustic coupling. The latter may be due to the fact that the chosen operating conditions may not fall within the discrete Strouhal bands. Such coupling has been studied recently in detail for a side branch on an engine induction system [31].

The results presented here are expected to somewhat depend on the design of the resonator, its location, the intake system, and the engine. It may also be expected, however, that the qualitative behavior and the trends presented in the study will remain applicable for similar elements in the intake system of internal combustion engines. While the use of "insertion loss" is extended to downstream locations of the silencer elements, an alternative wording for these locations such as "insertion impact" may possibly be more appropriate, as suggested in Ref. [25].

The predictions from a nonlinear fluid-dynamic (time-domain) model based on a finite difference approach compared reasonably well with the experiments. Thus, such a computational model is frequently used, in addition to engine performance predictions, to study the trends in terms of amplitudes and frequency components, reduce the number of alternatives, thereby accelerate the development process of intake/exhaust systems at the design stage. While the one-dimensional approach employed in the present study proves useful at relatively low airborne noise frequencies typical of internal combustion engine induction and exhaust systems, it currently faces the challenges of multi-dimensional propagation and the need for sound quality analysis.

## Appendix

This appendix discusses the effect of Helmholtz resonator on the pressure wave form and the corresponding sound pressure levels in the intake system at low (1000 rpm) and high (5000 rpm) engine speeds. Figs. 16 and 17 compare the pressure in the intake system with and without the Helmholtz resonator at intake primary runner locations 81 and 86, plenum 72, and the intake pipe locations 91, 92, and 93 for 1000 rpm. In the intake primary runners and the plenum (Fig. 16), insertion of the Helmholtz resonator changes the pressure wave form and increases the amplitude. At location 92 [downstream, Fig. 17(a)], the pressure wave forms are similar, but the amplitude is lower with the Helmholtz resonator in the intake system in comparison to the straight pipe. At locations 93 [neck, Fig. 17(b)] and 91 [upstream, Fig. 17(c)], similar to the intake manifold and primary runners, the pressure wave form changes and the amplitude is higher with the Helmholtz resonator compared to the straight pipe. The amplitude variation due to the insertion of resonator at this speed is consistent with the predictions presented in Fig. 15.

The crank-angle resolved pressure at 5000 rpm is shown in Figs. 18 and 19 for the intake system with and without the Helmholtz resonator. Unlike the 1000 and 1780 rpm, the pressure wave form as well as the amplitude in the intake manifold (Fig. 18), including the intake primary runners and the plenum, is nearly identical with and without the Helmholtz resonator. The intake pipe locations 92, 93, and 91 (Fig. 19), however, exhibit some differences in the pressure wave form and amplitude. The weakened impact at this speed is expected in view of the fact that the fundamental firing frequency is now 250 Hz, which is significantly above the effective frequency of the Helmholtz resonator. The resonator continues to reflect lower order less significant components corresponding to the design frequency, as will be discussed next with spectral information, thereby leading to a secondary effect on the pressure variation.

The sound pressure level versus order for the first few half and integer orders (up to 10th order) corresponding to the pressure-time data of Figs. 16–19 is given in Figs. 20–23. At 1000 rpm, the 3rd order in the intake manifold (Fig. 20) is dominant both with and without the Helmholtz resonator. The insertion of resonator increases $L_p$ at this order by about 10 dB. In the intake pipe location 92 at 1000 rpm [Fig. 21(a)], the 3rd, 6th, and 9th orders are significant with the straight pipe and the Helmholtz resonator, and the IL for these orders is positive. At locations 93 and 91 for the same engine speed, the IL for the 3rd order due to the Helmholtz resonator is negative. The IL at other orders may be neglected, since their contribution to the $L_{po}$ is insignificant because of low $L_p$. Note that the insertion loss for the $5\frac{1}{2}$ order at 1000 rpm (91.67 Hz) which nearly corresponds to the resonance frequency of the Helmholtz resonator is positive at all locations in the intake system. At 5000 rpm, Fig. 22 demonstrates that the $L_p$ in the intake manifold is nearly the same for most orders with and without the Helmholtz resonator. Note from Fig. 23 that the IL at 5000 rpm is significant in the intake pipe locations for the 1st order as this order nearly corresponds to 89 Hz. At locations 91 and 93, the IL is considerable for the lower orders (up to $2\frac{1}{2}$), while it is, in general, insignificant at higher orders.

## References

[1] Morse PM, Boden RH, Schecter H. Acoustic vibrations and internal combustion engine performance. I. Standing waves in the intake pipe system. Journal of Applied Physics 1938;9:16–23.
[2] Kastner LJ. Induction ramming effects in single cylinder four-stroke engine. IMechE 1945;153:206–20.
[3] Thompson MP, Engelman, HW. The two types of resonance in intake tuning. American Society of Engineers 69-DGP-11, 1969.
[4] Engelman HW. Design of a tuned intake manifold. American Society of Mechanical Engineers 73-WA/DGP-2, 1973.
[5] Rubayi NA. Acoustic vibrations in intake manifold system and the supercharging of engines. Applied Acoustics 1972;5:39–53.
[6] Ohata A, Ishida Y. Dynamic inlet pressure and volumetric efficiency of four cycle cylinder engine. SAE 820407, 1982.
[7] Jameson RT, Hodgins, PA. Improvement of the torque characteristics of a small, high speed engine through the design of Helmholtz-tuned manifoling. SAE 900680, 1990.
[8] Driels MR. dynamics of I.C. engine induction systems. Journal of Sound and Vibration 1975;43(3):499–510.
[9] Selamet A, Dickey NS, Novak JM. Theoretical, computational and experimental investigation of Helmholtz resonators with fixed volume: lumped versus distributed analysis. Journal of Sound and Vibration 1995;187(2):358–67.
[10] Eversman W. A systematic procedure for the analysis of multiply branched acoustic transmission lines. American Society of Mechanical Engineers 1987;109:168–77.
[11] Eversman W, White JA. Acoustic modelling and optimisation of induction system components. In: Proceedings of the 1995 Noise and Vibration Conference, P-291 Vol. 1, SAE 951261, pp. 207–215.
[12] Lamancusa JS. Geometric optimization of internal combustion engine induction systems for minimum noise transmission. Journal of Sound and Vibration 1988;127(2):303–18.
[13] Nishio Y, Kohama T, Kuroda O. New approach to low-noise air intake system development. SAE 911042, 1991.
[14] Kostun, JD, Lin JS. Effect of resonator location on resonator effectiveness using NASTRAN mode shape prediction analysis and LAMPS acoustic model. SAE 940614, 1994.
[15] Chapman M, Novak JM, Stein RA. A nonlinear acoustic model of inlet and exhaust flow in multicylinder internal combustion engines. American Society of Mechanical Engineers 83-WA/DSC-14, 1983.
[16] Matsumoto I, Ohata A. Variable induction systems to improve volumetric efficiency at low and/or medium engine speeds. SAE 860100, 1986.
[17] Pearson RJ, Winterbone DE. A rapid wave action simulation technique for intake manifold design. SAE 900676, 1990.
[18] Singh R, Soedel W. Mathematical modelling of multicylinder compressor discharge system interactions. Journal of Sound and Vibration 1979;63(1):125–43.
[19] Desantes JM, Torregrosa AJ, Broatch A. Hybrid linear/nonlinear method for exhaust noise prediction. SAE 950545, 1995.
[20] Munjal ML. Analysis and design of mufflers — an overview of research at Indian Institute of Science. Journal of Sound and Vibration 1998;211(3):425–33.
[21] Benson RS, Garg RD, Woollatt D. A numerical solution of unsteady flow problems. Int J Mech Sci 1964;6(1):117–44.
[22] Chapman M, Novak JM, Stein RA. Numerical modeling of inlet and exhaust flows in multi-cylinder internal combustion engines. In: Uzkan T. editor. Flows in internal combustion engines. Austin (TX): ASME WAM, 1982.
[23] Silvestri JJ, Morel T, Costello M. Study of intake wave dynamics and acoustics by simulation and experiment. SAE 940206, 1994.
[24] Stockhausen WF, Wiemero TA, Ives DC, Kronik AY. Development and application of the Ford split port induction system. SAE 961151, 1996.
[25] Selamet A, Kothamasu V, Novak JM, Kach RA. Experimental investigation of in-duct insertion loss of catalysts in internal combustion engines. Applied Acoustics 2000;60(4):451–87.

[26] Davis DD, Stokes GM, Moore D, Stevens GL. Theoretical and experimental investigation of mufflers with comments on engine-exhaust muffler design. National Advisory Committee for Aeronautics report no. 1192. 1954.
[27] Brigham EO. The fast Fourier transform and its application. Englewood Cliffs (NJ): Prentice Hall, 1988.
[28] Selamet A, Dickey NS, Novak JM. A time-domain computational simulation of acoustic silencers. Journal of Vibration and Acoustics 1995;117(3A):323–31.
[29] Gösele K. Das Dämpfungsverhalten von Reflexions-Schalldämpfern bei Luftgleischströmung. VDI-Berichte, 1965;88:123–30.
[30] Panton RL. Effect of orifice geometry on Helmholtz resonator excitation by grazing flow. AIAA Journal 1990;28(1):60–5.
[31] Selamet A, Kurniawan D, Knotts BD, Novak JM. Study of whistles with a generic sidebranch. In: Proceedings of 1999 SAE-Noise and Vibration Conference. SAE 1999-01-1814, 1999.